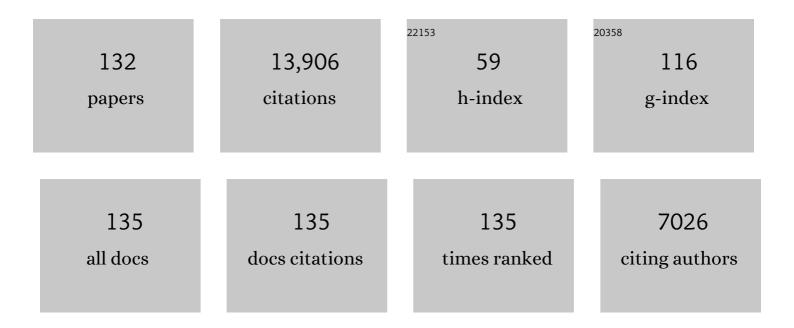
Simon W Poulton

List of Publications by Year in descending order

Source: https://exaly.com/author-pdf/1254899/publications.pdf Version: 2024-02-01



#	Article	IF	CITATIONS
1	A template for an improved rock-based subdivision of the pre-Cryogenian timescale. Journal of the Geological Society, 2022, 179, .	2.1	18
2	Insights from modern diffuse-flow hydrothermal systems into the origin of post-GOE deep-water Fe-Si precipitates. Geochimica Et Cosmochimica Acta, 2022, 317, 1-17.	3.9	2
3	A short-lived oxidation event during the early Ediacaran and delayed oxygenation of the Proterozoic ocean. Earth and Planetary Science Letters, 2022, 577, 117274.	4.4	18
4	Calibrating the temporal and spatial dynamics of the Ediacaran - Cambrian radiation of animals. Earth-Science Reviews, 2022, 225, 103913.	9.1	39
5	Carbonate shutdown, phosphogenesis and the variable style of marine anoxia in the late Famennian (Late Devonian) in western Laurentia. Palaeogeography, Palaeoclimatology, Palaeoecology, 2022, 589, 110835.	2.3	8
6	Extensive marine anoxia in the European epicontinental sea during the end-Triassic mass extinction. Global and Planetary Change, 2022, 210, 103771.	3.5	20
7	No effect of thermal maturity on the Mo, U, Cd, and Zn isotope compositions of Lower Jurassic organic-rich sediments. Geology, 2022, 50, 598-602.	4.4	16
8	Earth's Great Oxidation Event facilitated by the rise of sedimentary phosphorus recycling. Nature Geoscience, 2022, 15, 210-215.	12.9	26
9	Pyrite mega-analysis reveals modes of anoxia through geological time. Science Advances, 2022, 8, eabj5687.	10.3	11
10	A nutrient control on expanded anoxia and global cooling during the Late Ordovician mass extinction. Communications Earth & Environment, 2022, 3, .	6.8	17
11	Decoupled oxygenation of the Ediacaran ocean and atmosphere during the rise of early animals. Earth and Planetary Science Letters, 2022, 591, 117619.	4.4	17
12	Origin of the Neoarchean VMS-BIF Metallogenic Association in the Qingyuan Greenstone Belt, North China Craton: Constraints from Geology, Geochemistry, and Iron and Multiple Sulfur (<i>Ĩ´</i> 33S,) Tj ETQq0 0 0	rg ₿₮ /Ove	erlæck 10 Tf 5
13	Redox evolution and the development of oxygen minimum zones in the Eastern Mediterranean Levantine basin during the early Holocene. Geochimica Et Cosmochimica Acta, 2021, 297, 82-100.	3.9	10
14	A 200-million-year delay in permanent atmospheric oxygenation. Nature, 2021, 592, 232-236.	27.8	105
15	Pulsed oxygenation events drove progressive oxygenation of the early Mesoproterozoic ocean. Earth and Planetary Science Letters, 2021, 559, 116754.	4.4	28
16	Curation and Analysis of Global Sedimentary Geochemical Data to Inform Earth History. GSA Today, 2021, 31, 4-10.	2.0	9
17	The origin of early-Paleozoic banded iron formations in NW China. Gondwana Research, 2021, 93, 218-226.	6.0	3
18	lsotopic constraints on ocean redox at the end of the Eocene. Earth and Planetary Science Letters, 2021. 562. 116814.	4.4	6

#	Article	IF	CITATIONS
19	The Sedimentary Geochemistry and Paleoenvironments Project. Geobiology, 2021, 19, 545-556.	2.4	26
20	Limited expression of the Paleoproterozoic Oklo natural nuclear reactor phenomenon in the aftermath of a widespread deoxygenation event ~2.11–2.06 billion years ago. Chemical Geology, 2021, 578, 120315.	3.3	3
21	A chemical weathering control on the delivery of particulate iron to the continental shelf. Geochimica Et Cosmochimica Acta, 2021, 308, 204-216.	3.9	15
22	Arid climate disturbance and the development of salinized lacustrine oil shale in the Middle Jurassic Dameigou Formation, Qaidam Basin, northwestern China. Palaeogeography, Palaeoclimatology, Palaeoecology, 2021, 577, 110533.	2.3	15
23	Progressive development of ocean anoxia in the end-Permian pelagic Panthalassa. Global and Planetary Change, 2021, 207, 103650.	3.5	11
24	A Mississippian black shale record of redox oscillation in the Craven Basin, UK. Palaeogeography, Palaeoclimatology, Palaeoecology, 2020, 538, 109423.	2.3	11
25	Spatio-temporal evolution of ocean redox and nitrogen cycling in the early Cambrian Yangtze ocean. Chemical Geology, 2020, 554, 119803.	3.3	18
26	A nutrient control on marine anoxia during the end-Permian mass extinction. Nature Geoscience, 2020, 13, 640-646.	12.9	56
27	The biogeochemistry of ferruginous lakes and past ferruginous oceans. Earth-Science Reviews, 2020, 211, 103430.	9.1	36
28	Tracing water column euxinia in Eastern Mediterranean Sapropels S5 and S7. Chemical Geology, 2020, 545, 119627.	3.3	22
29	Development of Iron Speciation Reference Materials for Palaeoredox Analysis. Geostandards and Geoanalytical Research, 2020, 44, 581-591.	3.1	31
30	The origin and rise of complex life: progress requires interdisciplinary integration and hypothesis testing. Interface Focus, 2020, 10, 20200024.	3.0	13
31	Evaluating a primary carbonate pathway for manganese enrichments in reducing environments. Earth and Planetary Science Letters, 2020, 538, 116201.	4.4	42
32	Phosphorus-limited conditions in the early Neoproterozoic ocean maintained low levels of atmospheric oxygen. Nature Geoscience, 2020, 13, 296-301.	12.9	63
33	Unravelling the paleoecology of flat clams: New insights from an Upper Triassic halobiid bivalve. Global and Planetary Change, 2020, 190, 103195.	3.5	4
34	Molybdenum isotope and trace metal signals in an iron-rich Mesoproterozoic ocean: A snapshot from the Vindhyan Basin, India. Precambrian Research, 2020, 343, 105718.	2.7	18
35	Carbon isotopes in clastic rocks and the Neoproterozoic carbon cycle. Numerische Mathematik, 2020, 320, 97-124.	1.4	55
36	Copper and its Isotopes in Organic-Rich Sediments: From the Modern Peru Margin to Archean Shales. Geosciences (Switzerland), 2019, 9, 325.	2.2	10

#	Article	IF	CITATIONS
37	Development of a modified SEDEX phosphorus speciation method for ancient rocks and modern iron-rich sediments. Chemical Geology, 2019, 524, 383-393.	3.3	24
38	Chromium isotopes in marine hydrothermal sediments. Chemical Geology, 2019, 529, 119286.	3.3	19
39	Possible links between extreme oxygen perturbations and the Cambrian radiation of animals. Nature Geoscience, 2019, 12, 468-474.	12.9	96
40	Limited oxygen production in the Mesoarchean ocean. Proceedings of the National Academy of Sciences of the United States of America, 2019, 116, 6647-6652.	7.1	42
41	Controls on amorphous organic matter type and sulphurization in a Mississippian black shale. Review of Palaeobotany and Palynology, 2019, 268, 1-18.	1.5	20
42	Phosphorus cycling in Lake Cadagno, Switzerland: A low sulfate euxinic ocean analogue. Geochimica Et Cosmochimica Acta, 2019, 251, 116-135.	3.9	51
43	Stepwise Earth oxygenation is an inherent property of global biogeochemical cycling. Science, 2019, 366, 1333-1337.	12.6	85
44	Extending the applications of sediment profile imaging to geochemical interpretations using colour. Continental Shelf Research, 2019, 185, 16-22.	1.8	7
45	Oxygenation of the Mesoproterozoic ocean and the evolution of complex eukaryotes. Nature Geoscience, 2018, 11, 345-350.	12.9	124
46	A model for the oceanic mass balance of rhenium and implications for the extent of Proterozoic ocean anoxia. Geochimica Et Cosmochimica Acta, 2018, 227, 75-95.	3.9	66
47	Molybdenum record from black shales indicates oscillating atmospheric oxygen levels in the early Paleoproterozoic. Numerische Mathematik, 2018, 318, 275-299.	1.4	31
48	Ocean euxinia and climate change "double whammy―drove the Late Ordovician mass extinction. Geology, 2018, 46, 535-538.	4.4	148
49	Stepwise oxygenation of the Paleozoic atmosphere. Nature Communications, 2018, 9, 4081.	12.8	166
50	Shallow water anoxia in the Mesoproterozoic ocean: Evidence from the Bashkir Meganticlinorium, Southern Urals. Precambrian Research, 2018, 317, 196-210.	2.7	32
51	Did anoxia terminate Ediacaran benthic communities? Evidence from early diagenesis. Precambrian Research, 2018, 313, 134-147.	2.7	23
52	Early Palaeozoic ocean anoxia and global warming driven by the evolution of shallow burrowing. Nature Communications, 2018, 9, 2554.	12.8	56
53	The iron paleoredox proxies: A guide to the pitfalls, problems and proper practice. Numerische Mathematik, 2018, 318, 491-526.	1.4	174
54	Links between seawater paleoredox and the formation of sediment-hosted massive sulphide (SHMS) deposits — Fe speciation and Mo isotope constraints from Late Devonian mudstones. Chemical Geology, 2018, 490, 45-60.	3.3	19

#	Article	IF	CITATIONS
55	Aerobic iron and manganese cycling in a redox-stratified Mesoarchean epicontinental sea. Earth and Planetary Science Letters, 2018, 500, 28-40.	4.4	54
56	Early phosphorus redigested. Nature Geoscience, 2017, 10, 75-76.	12.9	31
57	Microfossils from the late Mesoproterozoic – early Neoproterozoic Atar/El MreÃ⁻ti Group, Taoudeni Basin, Mauritania, northwestern Africa. Precambrian Research, 2017, 291, 63-82.	2.7	69
58	Onset of the aerobic nitrogen cycle during the Great Oxidation Event. Nature, 2017, 542, 465-467.	27.8	114
59	Controls on the evolution of Ediacaran metazoan ecosystems: A redox perspective. Geobiology, 2017, 15, 516-551.	2.4	79
60	Biological regulation of atmospheric chemistry en route to planetary oxygenation. Proceedings of the United States of America, 2017, 114, E2571-E2579.	7.1	64
61	Anoxic development of sapropel S1 in the Nile Fan inferred from redox sensitive proxies, Fe speciation, Fe and Mo isotopes. Chemical Geology, 2017, 475, 24-39.	3.3	24
62	Fraction-specific controls on the trace element distribution in iron formations: Implications for trace metal stable isotope proxies. Chemical Geology, 2017, 474, 17-32.	3.3	18
63	The onset of widespread marine red beds and the evolution of ferruginous oceans. Nature Communications, 2017, 8, 399.	12.8	86
64	Marine oxygen production and open water supported an active nitrogen cycle during the Marinoan Snowball Earth. Nature Communications, 2017, 8, 1316.	12.8	25
65	Latest Permian carbonate carbon isotope variability traces heterogeneous organic carbon accumulation and authigenic carbonate formation. Climate of the Past, 2017, 13, 1635-1659.	3.4	18
66	A palaeoecological model for the late Mesoproterozoic – early Neoproterozoic Atar/El MreÃ⁻ti Group, Taoudeni Basin, Mauritania, northwestern Africa. Precambrian Research, 2017, 299, 1-14.	2.7	31
67	Potentially bioavailable iron delivery by iceberg-hosted sediments and atmospheric dust to the polar oceans. Biogeosciences, 2016, 13, 3887-3900.	3.3	65
68	The Bacteriohopanepolyol Inventory of Novel Aerobic Methane Oxidising Bacteria Reveals New Biomarker Signatures of Aerobic Methanotrophy in Marine Systems. PLoS ONE, 2016, 11, e0165635.	2.5	41
69	A multiproxy study distinguishes environmental change from diagenetic alteration in the recent sedimentary record of the inner Cadiz Bay (SW Spain). Holocene, 2016, 26, 1355-1370.	1.7	8
70	Repeated enrichment of trace metals and organic carbon on an Eocene high-energy shelf caused by anoxia and reworking. Geology, 2016, 44, 1011-1014.	4.4	19
71	Palaeoceanographic controls on spatial redox distribution over the Yangtze Platform during the Ediacaran–Cambrian transition. Sedimentology, 2016, 63, 378-410.	3.1	85
72	Black shale deposition and early diagenetic dolomite cementation during Oceanic Anoxic Event 1: The mid-Cretaceous Maracaibo Platform, northwestern South America. Numerische Mathematik, 2016, 316, 669-711.	1.4	18

#	Article	IF	CITATIONS
73	Trace elements at the intersection of marine biological and geochemical evolution. Earth-Science Reviews, 2016, 163, 323-348.	9.1	135
74	Open system sulphate reduction in a diagenetic environment – Isotopic analysis of barite (δ34S and δ18O) and pyrite (δ34S) from the Tom and Jason Late Devonian Zn–Pb–Ba deposits, Selwyn Basin, Canada. Geochimica Et Cosmochimica Acta, 2016, 180, 146-163.	3.9	77
75	Molybdenum drawdown during Cretaceous Oceanic Anoxic Event 2. Earth and Planetary Science Letters, 2016, 440, 81-91.	4.4	61
76	Determination of the stable iron isotopic composition of sequentially leached iron phases in marine sediments. Chemical Geology, 2016, 421, 93-102.	3.3	58
77	Multiple oscillations in Neoarchaean atmospheric chemistry. Earth and Planetary Science Letters, 2015, 431, 264-273.	4.4	67
78	A global transition to ferruginous conditions in the early Neoproterozoic oceans. Nature Geoscience, 2015, 8, 466-470.	12.9	105
79	The evolution of the global selenium cycle: Secular trends in Se isotopes and abundances. Geochimica Et Cosmochimica Acta, 2015, 162, 109-125.	3.9	59
80	Rise to modern levels of ocean oxygenation coincided with the Cambrian radiation of animals. Nature Communications, 2015, 6, 7142.	12.8	250
81	A continental-weathering control on orbitally driven redox-nutrient cycling during Cretaceous Oceanic Anoxic Event 2. Geology, 2015, 43, 963-966.	4.4	77
82	Selenium isotope evidence for progressive oxidation of the Neoproterozoic biosphere. Nature Communications, 2015, 6, 10157.	12.8	72
83	Dynamic redox conditions control late Ediacaran metazoan ecosystems in the Nama Group, Namibia. Precambrian Research, 2015, 261, 252-271.	2.7	134
84	Ocean acidification and the Permo-Triassic mass extinction. Science, 2015, 348, 229-232.	12.6	284
85	Phosphorus sources for phosphatic Cambrian carbonates. Bulletin of the Geological Society of America, 2014, 126, 145-163.	3.3	52
86	Phosphorus burial and diagenesis in the central Bering Sea (Bowers Ridge, IODP Site U1341): Perspectives on the marine P cycle. Chemical Geology, 2014, 363, 270-282.	3.3	40
87	Co-evolution of eukaryotes and ocean oxygenation in the Neoproterozoic era. Nature Geoscience, 2014, 7, 257-265.	12.9	305
88	Analysis of mass dependent and mass independent selenium isotope variability in black shales. Journal of Analytical Atomic Spectrometry, 2014, 29, 1648-1659.	3.0	23
89	Assessing the utility of Fe/Al and Fe-speciation to record water column redox conditions in carbonate-rich sediments. Chemical Geology, 2014, 382, 111-122.	3.3	181
90	Anaerobic ammonium-oxidising bacteria: A biological source of the bacteriohopanetetrol stereoisomer in marine sediments. Geochimica Et Cosmochimica Acta, 2014, 140, 50-64.	3.9	49

#	Article	IF	CITATIONS
91	Bioavailability of zinc in marine systems through time. Nature Geoscience, 2013, 6, 125-128.	12.9	84
92	Re–Os age constraints and new observations of Proterozoic glacial deposits in the Vazante Group, Brazil. Precambrian Research, 2013, 238, 199-213.	2.7	48
93	Surface charge and growth of sulphate and carbonate green rust in aqueous media. Geochimica Et Cosmochimica Acta, 2013, 108, 141-153.	3.9	90
94	Searching for an oxygenation event in the fossiliferous Ediacaran of northwestern Canada. Chemical Geology, 2013, 362, 273-286.	3.3	78
95	Redox changes in Early Cambrian black shales at Xiaotan section, Yunnan Province, South China. Precambrian Research, 2013, 225, 166-189.	2.7	116
96	Anoxia in the terrestrial environment during the late Mesoproterozoic. Geology, 2013, 41, 583-586.	4.4	75
97	Stability of the nitrogen cycle during development of sulfidic water in the redox-stratified late Paleoproterozoic Ocean. Geology, 2013, 41, 655-658.	4.4	57
98	Pathways for Neoarchean pyrite formation constrained by mass-independent sulfur isotopes. Proceedings of the National Academy of Sciences of the United States of America, 2013, 110, 17638-17643.	7.1	125
99	Green rust formation controls nutrient availability in a ferruginous water column. Geology, 2012, 40, 599-602.	4.4	159
100	Molybdenum isotope fractionations observed under anoxic experimental conditions. Geochemical Journal, 2012, 46, 201-209.	1.0	21
101	Controls on Mo isotope fractionations in a Mn-rich anoxic marine sediment, Gullmar Fjord, Sweden. Chemical Geology, 2012, 296-297, 73-82.	3.3	95
102	A bistable organic-rich atmosphere on the Neoarchaean Earth. Nature Geoscience, 2012, 5, 359-363.	12.9	201
103	Sedimentary phosphorus and iron cycling in and below the oxygen minimum zone of the northern Arabian Sea. Biogeosciences, 2012, 9, 2603-2624.	3.3	95
104	Molybdenum isotope constraints on the extent of late Paleoproterozoic ocean euxinia. Earth and Planetary Science Letters, 2011, 307, 450-460.	4.4	99
105	Does the Paleoproterozoic Animikie Basin record the sulfidic ocean transition?: COMMENT. Geology, 2011, 39, e241-e241.	4.4	5
106	Ferruginous Conditions: A Dominant Feature of the Ocean through Earth's History. Elements, 2011, 7, 107-112.	0.5	717
107	Spatial variability in oceanic redox structure 1.8 billion years ago. Nature Geoscience, 2010, 3, 486-490.	12.9	338
108	Pervasive oxygenation along late Archaean ocean margins. Nature Geoscience, 2010, 3, 647-652.	12.9	233

#	Article	IF	CITATIONS
109	An 80 million year oceanic redox history from Permian to Jurassic pelagic sediments of the Mino-Tamba terrane, SW Japan, and the origin of four mass extinctions. Global and Planetary Change, 2010, 71, 109-123.	3.5	172
110	An emerging picture of Neoproterozoic ocean chemistry: Insights from the Chuar Group, Grand Canyon, USA. Earth and Planetary Science Letters, 2010, 290, 64-73.	4.4	194
111	Fluctuations in Precambrian atmospheric oxygenation recorded by chromium isotopes. Nature, 2009, 461, 250-253.	27.8	554
112	Mo isotope fractionation during adsorption to Fe (oxyhydr)oxides. Geochimica Et Cosmochimica Acta, 2009, 73, 6502-6516.	3.9	248
113	Ferruginous Conditions Dominated Later Neoproterozoic Deep-Water Chemistry. Science, 2008, 321, 949-952.	12.6	626
114	Tracing the stepwise oxygenation of the Proterozoic ocean. Nature, 2008, 452, 456-459.	27.8	883
115	Redox sensitivity of P cycling during marine black shale formation: Dynamics of sulfidic and anoxic, non-sulfidic bottom waters. Geochimica Et Cosmochimica Acta, 2008, 72, 3703-3717.	3.9	196
116	Turbidite depositional influences on the diagenesis of Beecher's Trilobite Bed and the Hunsruck Slate; sites of soft tissue pyritization. Numerische Mathematik, 2008, 308, 105-129.	1.4	97
117	Late-Neoproterozoic Deep-Ocean Oxygenation and the Rise of Animal Life. Science, 2007, 315, 92-95.	12.6	812
118	Co-diagenesis of iron and phosphorus in hydrothermal sediments from the southern East Pacific Rise: Implications for the evaluation of paleoseawater phosphate concentrations. Geochimica Et Cosmochimica Acta, 2006, 70, 5883-5898.	3.9	70
119	Evolution of the oceanic sulfur cycle at the end of the Paleoproterozoic. Geochimica Et Cosmochimica Acta, 2006, 70, 5723-5739.	3.9	102
120	Development of a sequential extraction procedure for iron: implications for iron partitioning in continentally derived particulates. Chemical Geology, 2005, 214, 209-221.	3.3	932
121	Chemical and physical characteristics of iron oxides in riverine and glacial meltwater sediments. Chemical Geology, 2005, 218, 203-221.	3.3	139
122	Sulphur and oxygen isotope signatures of late Neoproterozoic to early Cambrian sulphate, Yangtze Platform, China: Diagenetic constraints and seawater evolution. Precambrian Research, 2005, 137, 223-241.	2.7	103
123	The transition to a sulphidic ocean â^¼ 1.84 billion years ago. Nature, 2004, 431, 173-177.	27.8	405
124	A revised scheme for the reactivity of iron (oxyhydr)oxide minerals towards dissolved sulfide. Geochimica Et Cosmochimica Acta, 2004, 68, 3703-3715.	3.9	490
125	Sulfide oxidation and iron dissolution kinetics during the reaction of dissolved sulfide with ferrihydrite. Chemical Geology, 2003, 202, 79-94.	3.3	164
126	Detection and removal of dissolved hydrogen sulphide in flowâ€ŧhrough systems via the sulphidation of hydrous iron (III) oxides. Environmental Technology (United Kingdom), 2003, 24, 217-229.	2.2	9

#	Article	IF	CITATIONS
127	The use of hydrous iron (III) oxides for the removal of hydrogen sulphide in aqueous systems. Water Research, 2002, 36, 825-834.	11.3	78
128	In-situ determination of dissolved iron production in recent marine sediments. , 2002, 64, 282-291.		40
129	Solid phase associations, oceanic fluxes and the anthropogenic perturbation of transition metals in world river particulates. Marine Chemistry, 2000, 72, 17-31.	2.3	43
130	Porewater sulphur geochemistry and fossil preservation during phosphate diagenesis in a Lower Cretaceous shelf mudstone. Sedimentology, 1998, 45, 875-887.	3.1	15
131	The Ediacaran â€ [~] Miaohe Member' of South China: new insights from palaeoredox proxies and stable isotope data. Geological Magazine, 0, , 1-15.	1.5	3
132	Combining Nitrogen Isotopes and Redox Proxies Strengthens Paleoenvironmental Interpretations: Examples From Neoproterozoic Snowball Earth Sediments. Frontiers in Earth Science, 0, 10, .	1.8	2